



Deep Ocean Impact of a Madden-Julian Oscillation Observed by Argo Floats

Adrian J. Matthews, *et al.*
Science **318**, 1765 (2007);
DOI: 10.1126/science.1147312

**The following resources related to this article are available online at
www.sciencemag.org (this information is current as of December 14, 2007):**

Updated information and services, including high-resolution figures, can be found in the online version of this article at:

<http://www.sciencemag.org/cgi/content/full/318/5857/1765>

Supporting Online Material can be found at:

<http://www.sciencemag.org/cgi/content/full/318/5857/1765/DC1>

A list of selected additional articles on the Science Web sites **related to this article** can be found at:

<http://www.sciencemag.org/cgi/content/full/318/5857/1765#related-content>

This article **cites 25 articles**, 2 of which can be accessed for free:

<http://www.sciencemag.org/cgi/content/full/318/5857/1765#otherarticles>

This article appears in the following **subject collections**:

Oceanography

<http://www.sciencemag.org/cgi/collection/oceans>

Information about obtaining **reprints** of this article or about obtaining **permission to reproduce this article** in whole or in part can be found at:

<http://www.sciencemag.org/about/permissions.dtl>

Pacific Ocean. Behind the leading edge, counterclockwise and clockwise vortices were generated at the equator and at 15°S, respectively, at around 120°E. The clockwise vortex northwest of Australia corresponded well with a real tropical cyclone named Isobel. The 7-km grid run successfully predicted this tropical cyclone at the proper location and time, even after the integration continued for more than 2 weeks.

On 2 January 2007, a smaller cloud system was simulated at around 105°E in association with a clockwise vortex (Fig. 4B). This clockwise vortex near the south end of Sumatra originated from a tropical depression-type (TD-type) disturbance (21), which changed its direction from westward to eastward west of 90°E around 29 December 2006 (Fig. 3, C and D). As the negative-vorticity region proceeded eastward, a rainband system began to grow around 130°E, traveled to the northwest of New Guinea, and developed into a mature system at around 148°E on 6 January 2007 (Fig. 4D). Around 6 January 2007, a large amount of moisture northeast of New Guinea provided suitable atmospheric conditions for the growth of cloud systems (Fig. 4C). Moisture was transported mainly from the central Pacific, where the SST was as warm as in the western Pacific because of an El Niño event (fig. S3). The eastward-propagating rainband system brought low-level cool air into the South Pacific Convergence Zone (fig. S2), and the convective center of the MJO shifted from the maritime continents to the Pacific Ocean. Rainband systems northeast of New Guinea were also observed in the other MJO events during TOGA-COARE IOP (Tropical Ocean Global Atmosphere–Coupled Ocean Atmosphere Response Experiment, Intensive Observation Period) from November 1992 to February 1993 (22, 23).

Overall, the 7-km grid run realistically reproduced the slow eastward migration of the MJO from the Indian to the Pacific Ocean. However, some features could have caused errors in the movement speed of the MJO. The 7-km grid run failed to simulate individual clouds correctly during the month-long integration. The zonal wind velocity tended to be overestimated over the tropics, and the effect of the overvalued surface precipitation might result in inaccuracy in the estimated amount of latent heat release. Despite these imperfections, the leading edge of the active convective envelope was positioned almost identically to that of observational data sets after the integration of more than 3 weeks on 6 January 2007. A possible explanation for the good correspondence between the 7-km grid run and observations is that the temporal evolution of the MJO is dominated by large-scale systems that the 7-km grid can resolve sufficiently. As inferred from the results of resolution-sensitivity studies using cloud-resolving models in limited domains (24, 25), GCRMs probably have the ability to respond to a given large-scale forcing and restore statistical equilibrium states in a realistic time scale, even if a coarse horizontal resolution is used.

Our results demonstrate the potential ability of GCRMs to make month-long MJO predictions when they run with realistic initial conditions. The principal factors governing the realistic eastward migration of the MJO were the interference of preceding rainband systems from New Guinea and drier air over an area with a relatively cool SST, an eastward-propagating signal that originated from a TD-type disturbance, and abundant moisture supply from the east, probably in association with a westward-propagating disturbance. These results support the hypothesis derived from analyses of the TRMM (Tropical Rainfall Measuring Mission) data, which showed that a group of eastward-propagating Kelvin waves and their interaction with westward-propagating equatorial Rossby waves play a crucial role in MJOs (26); and they emphasize the influence of topography and the zonal SST gradient on the MJO.

References and Notes

- R. A. Madden, P. R. Julian, *J. Atmos. Sci.* **29**, 1109 (1972).
- D. E. Waliser, K. M. Lau, W. Stern, C. Jones, *Bull. Am. Meteorol. Soc.* **84**, 33 (2003).
- C. Zhang, *Rev. Geophys.* **43**, RG2003 (2005).
- J. M. Slingo *et al.*, *Clim. Dyn.* **12**, 325 (1996).
- J.-L. Lin *et al.*, *J. Clim.* **19**, 2665 (2006).
- E. D. Maloney, D. L. Hartmann, *J. Clim.* **14**, 2015 (2001).
- R. A. Kerr, *Science* **313**, 1040 (2006).
- W. W. Grabowski, *J. Atmos. Sci.* **60**, 847 (2003).
- M. F. Khairoutdinov, D. A. Randall, C. DeMotte, *J. Atmos. Sci.* **62**, 2136 (2005).
- A. Arakawa, W. H. Schubert, *J. Atmos. Sci.* **31**, 674 (1974).
- M. Satoh *et al.*, *J. Comput. Phys.*, published online 17 February 2007, 10.1016/j.jcp.2007.02.006.
- H. Tomita, H. Miura, S. Iga, T. Nasuno, M. Satoh, *Geophys. Res. Lett.* **32**, L08805 (2005).
- H. Miura *et al.*, *Geophys. Res. Lett.* **32**, L19717 (2005).
- H. Miura *et al.*, *Geophys. Res. Lett.* **34**, L02804 (2007).
- The other experimental settings followed the realistic tropical cyclone experiment (14), except for updating a boundary-layer scheme to include a partial condensation process (27) and introducing a monotone advection scheme (28).
- T. Nakazawa, *J. Meteorol. Soc. Jpn.* **66**, 823 (1988).
- H. H. Hendon, B. Liebmann, *J. Geophys. Res.* **99**, 8073 (1994).
- T. Matsuno, *J. Meteorol. Soc. Jpn.* **44**, 25 (1966).
- Y. N. Takayabu, *J. Meteorol. Soc. Jpn.* **72**, 433 (1994).
- M. Wheeler, G. N. Kiladis, *J. Atmos. Sci.* **56**, 374 (1999).
- Y. N. Takayabu, T. Niita, *J. Meteorol. Soc. Jpn.* **71**, 221 (1993).
- N. Takahashi, H. Uyeda, *J. Meteorol. Soc. Jpn.* **73**, 427 (1995).
- S. Satoh, A. Kinoshita, H. Uyeda, *J. Meteorol. Soc. Jpn.* **73**, 443 (1995).
- W. W. Grabowski, X. Wu, M. W. Moncrieff, W. D. Hall, *J. Atmos. Sci.* **55**, 3264 (1998).
- M. F. Khairoutdinov, D. A. Randall, *J. Atmos. Sci.* **60**, 607 (2003).
- H. Masunaga, T. S. L'ecuyer, C. D. Kummerow, *J. Atmos. Sci.* **63**, 2777 (2006).
- G. L. Mellor, T. Yamada, *Rev. Geophys. Space Phys.* **20**, 851 (1982).
- H. Miura, *Mon. Weather Rev.* **135**, 4038 (2007).
- This study was supported by Core Research for Evolutional Science and Technology of the Japan Science and Technology Agency (CREST, JST). The simulations were performed with the Earth Simulator at the Earth Simulator Center of the Japan Agency for Marine-Earth Science and Technology. We thank T. Matsuno, A. Sumi, M. Kimoto, Y. N. Takayabu, H. Tomita, and S. Iga for their advice and comments and T. Inoue, A. Higuchi, and S. Ishikawa for their help in treating the Multi-Functional Transport Satellite (MTSAT-1R) data.

Supporting Online Material

www.sciencemag.org/cgi/content/full/318/5857/1763/DC1
Figs. S1 to S3

27 July 2007; accepted 26 October 2007
10.1126/science.1148443

Deep Ocean Impact of a Madden-Julian Oscillation Observed by Argo Floats

Adrian J. Matthews,^{1,2*} Patama Singhruck,¹ Karen J. Heywood¹

Using the new Argo array of profiling floats that gives unprecedented space-time coverage of the upper 2000 meters of the global ocean, we present definitive evidence of a deep tropical ocean component of the Madden-Julian Oscillation (MJO). The surface wind stress anomalies associated with the MJO force eastward-propagating oceanic equatorial Kelvin waves that extend downward to 1500 meters. The amplitude of the deep ocean anomalies is up to six times the amplitude of the observed annual cycle. This deep ocean sink of energy input from the wind is potentially important for understanding phenomena such as El Niño–Southern Oscillation and for interpreting deep ocean measurements made from ships.

The Madden-Julian Oscillation (MJO) (1–3) is characterized by large-scale (1000 km across) precipitation anomalies that propagate slowly eastward from the Indian Ocean to the western Pacific. The lifetime of an individual MJO event is between 30 and 60 days. Dynamically, the MJO can be interpreted as a moist atmospheric Kelvin-Rossby wave in the tropics (4) and a modified Rossby wave response

propagating on the climatological basic state in the extratropics (5). The MJO is thermodynamically coupled with the upper layers of the tropical

¹School of Environmental Sciences, University of East Anglia, Norwich NR4 7TJ, UK. ²School of Mathematics, University of East Anglia, Norwich NR4 7TJ, UK.

*To whom correspondence should be addressed. E-mail: a.j.matthews@uea.ac.uk

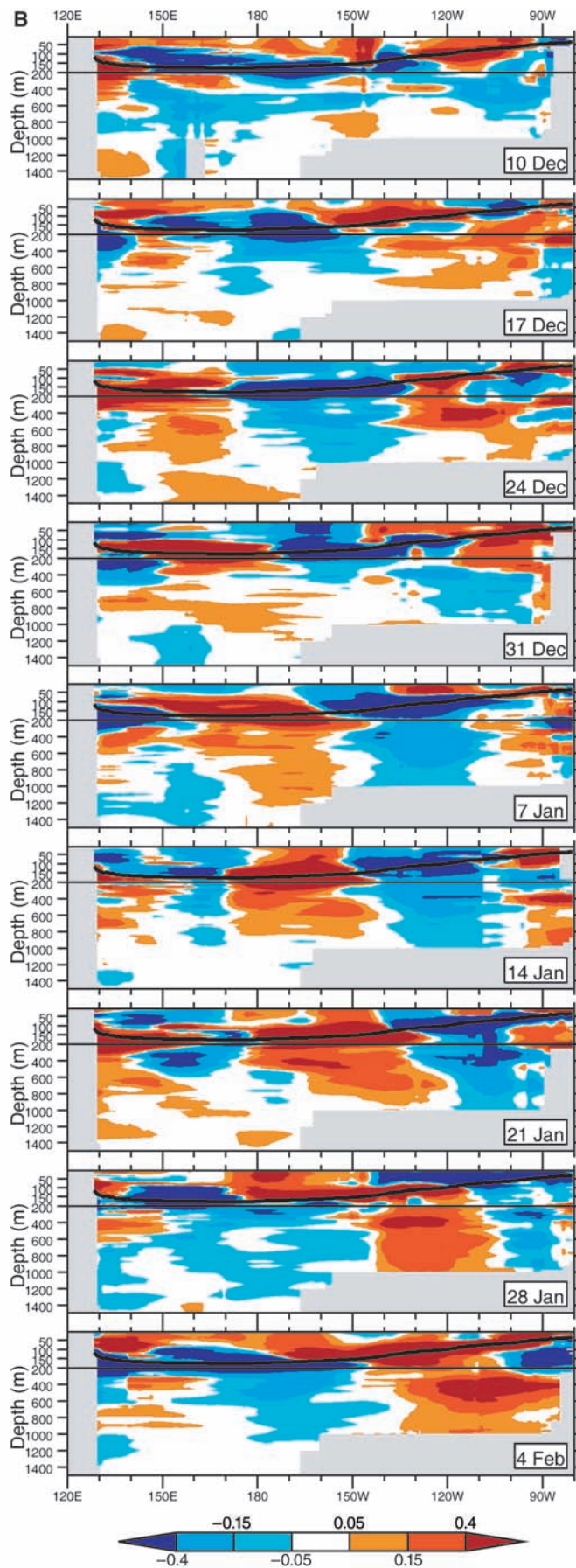
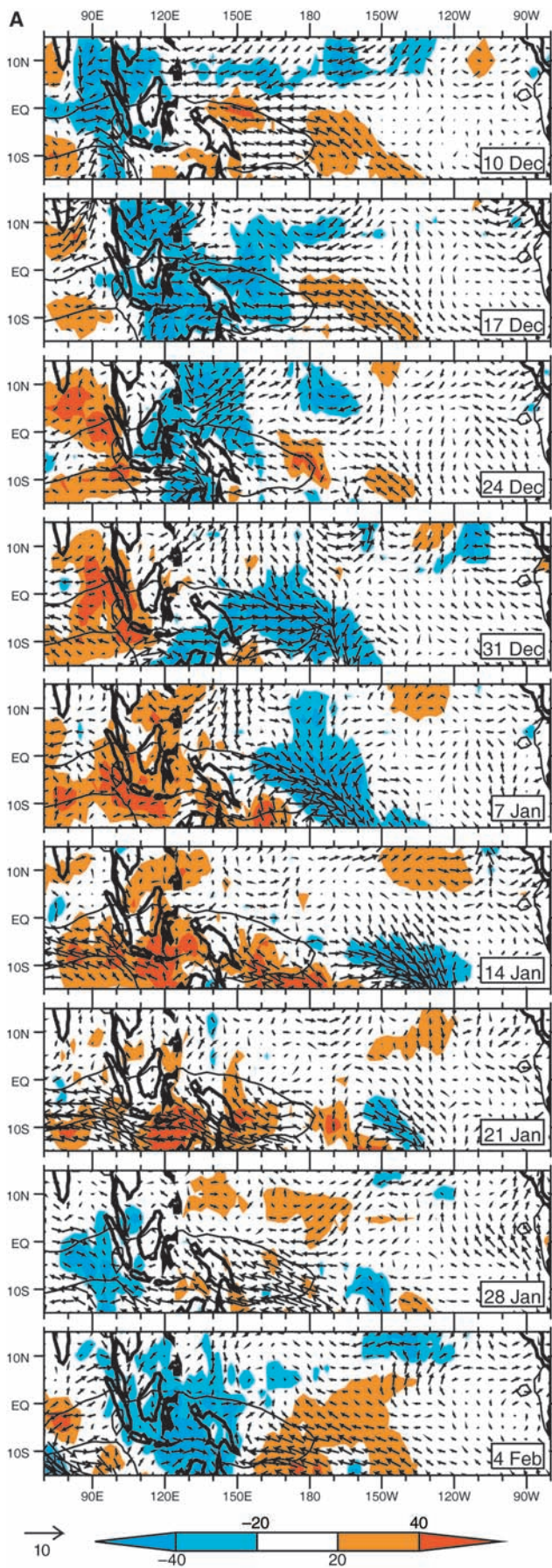


Fig. 1 (opposite page). Weekly mean anomalies (annual cycle subtracted) from 10 December 2003 to 4 February 2004 in the western Pacific. **(A)** OLR. Shading interval is 20 W m^{-2} (see scale bar); wind vectors are 1000 hPa. The length of the vector arrows is proportional to the magnitude of the wind vector. The standard wind vector in the lower left corner has magnitude 10 m s^{-1} . The zero climatological-mean zonal wind contour is shown by a solid line. **(B)** Longitude-depth sections of Argo temperature along the equator (averaged 5°S to 5°N). Note the change of vertical scale at 200 m. Contours are at $\pm 0.05^{\circ}$, 0.15° , and 0.4°C (see scale bar). The depth of the mean thermocline (20°C isotherm) is shown by the thick line.

Indian and Pacific oceans (6–8). Anomalous surface fluxes of shortwave (solar) radiation due to cloudiness changes, and latent heat due to evaporation from the ocean surface through surface wind speed changes, both heat and cool the ocean mixed layer by up to 1°C in a strong MJO event (6).

In addition, oceanic equatorial Kelvin waves in the central and eastern Pacific are forced by MJO wind stress anomalies (9–12). A sequence of MJO events can force a train of eastward-propagating equatorial Kelvin waves along the thermocline in the Pacific, which can trigger an El Niño event (13, 14) such as the event of 1997–1998 (15, 16). The MJO has a direct impact on the ocean biosphere: The MJO-forced oceanic Kelvin waves modulate the surface chlorophyll concentration through vertical entrainment, with implications for the fishing industry (17).

The upper tropical ocean component of the MJO has been well documented (6–8), but the data have not been available to examine whether there is a deep tropical ocean component. The deepest MJO-linked observations in the tropical ocean—from the Tropical Atmosphere Ocean (TAO) moored buoy network in the tropical Pacific—extend down to only 500 m (9). A 50-day oscillation has been observed in currents down to 3000 m depth in the Indian Ocean, consistent with a zonally propagating Rossby wave (18), but these limited data have not been linked to the MJO or any atmospheric surface forcing. However, the MJO can influence the deep ocean in high latitudes (19).

Therefore, it seems plausible that the MJO may influence the deep ocean in the tropics, but the limited hydrographic data that exist do not have the temporal resolution necessary for an analysis of intraseasonal variability. However, this situation has begun to change because of the advent of the Argo ocean observing system (20). Argo floats have been deployed since 2000 and are at the core of current efforts to set up a global ocean observing system (21). Today almost 3000 floats are operational, providing unprecedented global coverage of the world oceans. Each float drifts at a typical parking depth of 1000 m for ~ 10 days. In ~ 2 hours, it then de-

Fig. 2. Longitude-time section (Hovmöller diagram) of equatorial (averaged 5°S to 5°N) Argo temperature anomaly at the 850-dbar level. Contour interval is 0.05°C (see scale bar). The thick solid line indicates the phase propagation of the downwelling Kelvin wave.

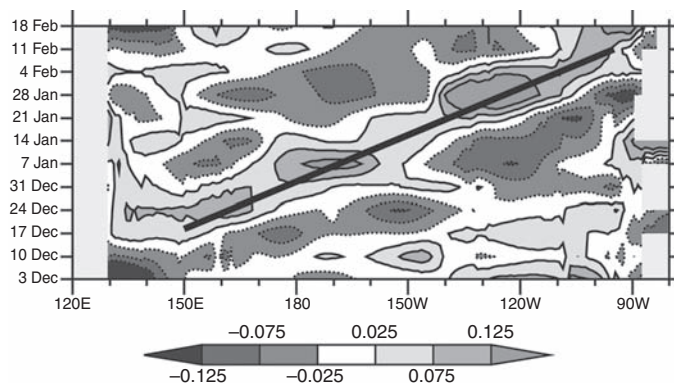
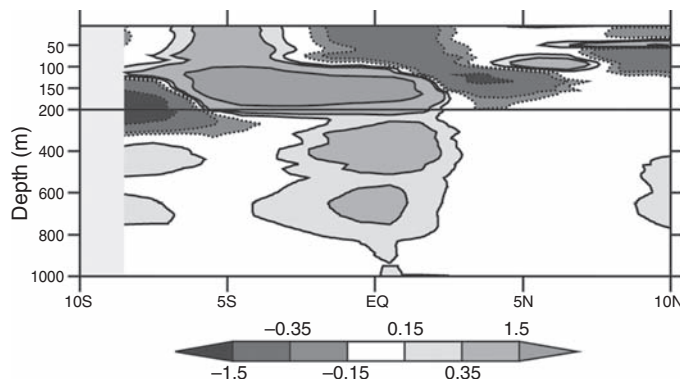


Fig. 3. Latitude-depth section of weekly mean Argo temperature anomaly at 140°W on 21 January 2004. Contours are at $\pm 0.15^{\circ}$, 0.35° , and 1.5°C (see scale bar).



scends to 2000 m, ascends to the surface, measuring a vertical profile of temperature and salinity, then descends again to its parking depth. Argo data have already been used to study mid-depth circulation at high latitudes (22) and seasonal temperature variation below the thermocline in the Pacific (23). The 10-day temporal resolution provides a new opportunity to study the spatial variability of the deep ocean on intraseasonal time scales.

Here, we used Argo data to reveal the oceanic component of the MJO downward into the deep Pacific, in a case study of the December 2003–February 2004 MJO event. Outgoing longwave radiation (OLR) was used as a proxy for precipitation (24), as low values of OLR are indicative of deep clouds and precipitation in the tropics. In the uppermost panel of Fig. 1A, which shows the Argo data for 10 December 2003, the positive OLR anomalies over the western Pacific indicate reduced precipitation (dry phase of MJO) with easterly surface wind anomalies, and the negative OLR anomalies over the eastern Indian Ocean indicate enhanced precipitation (wet phase of MJO) with equatorial westerly wind anomalies. A further region of positive OLR anomalies over the central Indian Ocean indicates the next dry phase of the MJO. These precipitation anomalies then propagate slowly eastward. The 56-day period shown in Fig. 1A covers slightly more than one full cycle of the MJO.

The MJO exerts a thermodynamical control on the ocean mixed layer via changes to the

surface shortwave and latent heat fluxes. Negative OLR anomalies imply more deep clouds, a reduction in the downward surface shortwave flux, and a cooling of the ocean surface. Intraseasonal latent heat flux (evaporation) anomalies are mainly controlled by changes in the total (climatological mean plus anomalous) surface wind speed. West of the date line, westerly surface wind anomalies reinforce the mean westerlies there (Fig. 1A). The total wind speed will increase, increasing evaporation from the ocean surface and cooling it. East of the date line, westerly anomalies partially cancel the mean easterlies, reducing the total wind speed and evaporation and providing a warming anomaly to the ocean. The sea surface temperature (SST) response to these changes in the surface fluxes is lagged by approximately one-quarter of the MJO cycle, or 1 to 2 weeks (6).

The surface shortwave and latent heat flux anomalies lead to changes in the equatorial western Pacific SST throughout this particular MJO event, as clearly illustrated by the gridded Argo temperature anomalies (24). Initially, the positive SST anomalies in the equatorial western Pacific on 10 December (Fig. 1B) are due to the dry MJO phase and increased downward surface shortwave flux, as well as the reduction in evaporation and upward latent heat flux from the anomalous easterlies weakening the total wind speed, over the previous week. These flux anomalies are still present on 10 December, and a week later, on 17 December, there are still

positive SST anomalies over the western Pacific. However, the wet phase of the MJO has now moved over the western Pacific. The associated reduction in the downward surface shortwave flux, and the increased evaporation from surface westerlies enhancing the mean winds, lead to negative SST anomalies there from 24 December 2003 to 14 January 2004. When the next dry phase of the MJO arrives around 7 January, the flux anomalies begin to change sign and positive SST anomalies return from 28 January onward.

The SST anomalies in the equatorial western Pacific that are consistent with thermodynamical forcing by the surface flux anomalies extend down through the mixed layer to about 50 m depth (Fig. 1B). Below this depth, the new Argo data set allows us to document the dynamical ocean mechanisms that become important below the mixed layer. On 10 December, the negative SST anomalies between 100 and 200 m in the western and central Pacific show an upwelling oceanic equatorial Kelvin wave that has arisen as a forced response to the surface easterly wind stress anomalies above. With the arrival of the wet phase of the MJO over the western Pacific on 17 December, the associated surface westerly anomalies (a “westerly wind burst”) begin to force a downwelling oceanic equatorial Kelvin wave, with a small region of positive SST anomalies at thermocline depth (180 m; thick line in Fig. 1B) at 150°E. These positive and negative temperature anomalies at the thermocline also extend coherently downward into the deeper ocean, to around 600 m.

By 24 December, the upwelling and downwelling Kelvin waves have propagated eastward along the thermocline. The largest-amplitude Argo temperature anomalies follow the thermocline, as this is the level of greatest vertical temperature gradient. The coherent temperature anomalies extend from the thermocline down to 1500 m, the deepest level of observations. From 31 December to 4 February, the upwelling and downwelling Kelvin waves continue to propagate eastward and also extend downward to at least 1200 m. The deep anomalies have a large amplitude. The maximum anomaly observed at 600 m is 0.45°C (on 4 February at 105°W); at 850 m, the maximum anomaly is 0.25°C (on 28 January at 130°W). These are greater by a factor of 3 to 6 than the amplitude of the annual cycle, which is 0.08° and 0.07°C at these locations, respectively, as calculated from the Argo data (24). Their amplitudes are also larger than the predicted deep ocean Kelvin wave response to intraseasonal wind forcing in an ocean model (25).

When the next dry phase of the MJO arrives over the western Pacific on 14 January (Fig. 1A), its easterly surface wind stress anomalies force another upwelling equatorial Kelvin wave. The associated negative temperature anomalies then propagate eastward along the thermocline and extend down to 1300 m (Fig. 1B).

The coherent eastward propagation of the upwelling, downwelling, and second upwelling phases of the deep Kelvin wave can be clearly seen in Hovmöller diagrams of the temperature anomalies in the deep ocean at 850 dbar (Fig. 2) and in the thermocline at 150 dbar (fig. S1). The average phase speed of the waves (slope of solid lines in Fig. 2 and fig. S1) is $c = 2.8 \text{ m s}^{-1}$, consistent with the typical observed phase speed of first-internal-mode equatorial Kelvin waves on the thermocline (12, 26). The vertical tilt of the anomalies can clearly be seen in a comparison of the two Hovmöller diagrams; the temperature anomalies in the thermocline (fig. S1) lead those in the deep ocean (Fig. 2) by a quarter cycle. The latitude-depth section of the temperature anomalies (Fig. 3) shows the characteristic spatial structure of a theoretical equatorial Kelvin wave. This has a maximum at the equator, then decays toward the poles with a Gaussian structure, $\exp(-\beta y^2/2c)$, where y is distance northward from the equator, and $\beta = 2.3 \times 10^{-11} \text{ m}^{-1} \text{ s}^{-1}$ is the latitudinal gradient of planetary vorticity. Using the observed value of $c = 2.8 \text{ m s}^{-1}$, we find that the latitudinal trapping scale is $y_0 = (2c/\beta)^{1/2} = 490 \text{ km} \approx 4.4^\circ$ latitude. This is consistent with the observed latitudinal structure of the deep Argo temperature anomalies in Fig. 3.

The vertical structure of the waves can be interpreted in terms of standing and vertically (downward) propagating components. The vertical phase lines (or, equivalently, zero-anomaly contours) in, for example, the eastern Pacific on 7 January indicate a standing component. Conversely, the phase line (zero-anomaly contour) that tilts downward and eastward in the eastern Pacific on 21 January indicates downward (energy) propagation of the Kelvin wave (27, 28), with a vertical wavelength of about 800 m, which is consistent with the theoretical value (24). Alternatively, the tilted phase lines and apparent vertical propagation can be interpreted as a superposition of vertical modes. However, in the Pacific, vertical modes of order 3 and higher are all subjected to critical layer dissipation in the equatorial undercurrent (25), and the deep structure is consistent with wave-mean flow interaction effects superimposed on a first-mode baroclinic structure.

The Argo data have facilitated an unprecedented view of the deep tropical Pacific Ocean on short (intraseasonal) time scales. This had not previously been possible, as conventional hydrographic data have inadequate time resolution and spatial coverage, and the TAO moored buoy network has a maximum depth of only 500 m. The MJO has been shown to force eastward-propagating equatorial Kelvin waves that extend downward into the deep ocean. Although intraseasonal Kelvin waves have been well studied in the near-surface layers (9, 25, 26), there has been no opportunity to observe the deeper signal until now. These Argo-observed

deep ocean Kelvin waves have larger amplitude than the annual cycle and model predictions, and they could potentially increase the errors in vertical structure, circulation, and heat content from hydrographic sections (29) if a Kelvin wave passed through at the time of the section. The anomalies in the deep (e.g., 600 m) geostrophic zonal currents, calculated from the Argo temperature and salinity data, are typically 1 cm s^{-1} . This is the same magnitude as the mean geostrophic current at these depths (below the equatorial undercurrent). Hence, these anomalies are a large perturbation to the mean currents and represent a substantial transfer of energy from the surface, where they are forced, to the deep ocean, where they must be dissipated.

The propagation of the Kelvin wave into the deep ocean will have effects on deep ocean biology and chemistry, and should be included in coupled models of the MJO. Furthermore, these deep ocean Kelvin waves will have an impact on ocean circulation outside the equatorial wave guide. Upon reaching the eastern boundary, the equatorial Kelvin wave will trigger meridionally propagating coastal Kelvin waves along the coastline of the Americas, which will then trigger westward-propagating Rossby waves back into the ocean interior.

References and Notes

- R. A. Madden, P. R. Julian, *Mon. Weather Rev.* **122**, 814 (1994).
- C. Zhang, *Rev. Geophys.* **43**, RG2003 (2005).
- W. K. M. Lau, D. E. Waliser, Eds., *Intraseasonal Variability in the Atmosphere-Ocean Climate System* (Springer-Praxis, Berlin, 2005).
- H. H. Hendon, M. L. Salby, *J. Atmos. Sci.* **53**, 1751 (1996).
- A. J. Matthews, B. J. Hoskins, M. Masutani, *Q. J. R. Meteorol. Soc.* **130**, 1991 (2004).
- T. Shinoda, H. H. Hendon, J. Glick, *J. Clim.* **11**, 1685 (1998).
- S. J. Woolnough, J. M. Slingo, B. J. Hoskins, *J. Clim.* **13**, 2086 (2000).
- M. J. McPhaden, *J. Clim.* **15**, 2632 (2002).
- W. S. Kessler, M. J. McPhaden, K. M. Weickmann, *J. Geophys. Res.* **100**, 10613 (1995).
- H. H. Hendon, B. Liebmann, J. D. Glick, *J. Atmos. Sci.* **55**, 88 (1998).
- C. Zhang, *J. Clim.* **14**, 1309 (2001).
- P. E. Roundy, G. N. Kiladis, *J. Clim.* **19**, 5253 (2006).
- C. Zhang, J. Gottschalck, *J. Clim.* **15**, 2429 (2002).
- K. H. Seo, Y. Xue, *Geophys. Res. Lett.* **32**, L07712 (2005).
- M. J. McPhaden, *Science* **283**, 950 (1999).
- K. Kutsuwada, M. J. McPhaden, *J. Phys. Oceanogr.* **32**, 1133 (2002).
- D. E. Waliser, R. Murtugudde, P. Strutton, J. L. Li, *Geophys. Res. Lett.* **32**, L23602 (2005).
- K. J. Heywood, E. D. Barton, G. L. Allen, *Oceanol. Acta* **17**, 255 (1994).
- A. J. Matthews, M. P. Meredith, *Geophys. Res. Lett.* **31**, L24312 (2004).
- J. Gould, *Eos* **85**, 190 (2004).
- K. Alverson, D. J. Baker, *Science* **314**, 1657 (2006).
- K. L. Lavender, R. E. Davis, W. B. Owens, *Nature* **407**, 66 (2000).
- S. Hosoda, S. Minato, N. Shikama, *Geophys. Res. Lett.* **33**, L13604 (2006).
- See supporting material on Science Online.
- E. S. Johnson, M. J. McPhaden, *J. Phys. Oceanogr.* **23**, 608 (1993).

26. S. Cravatte, J. Picaut, G. Eldin, *J. Geophys. Res.* **108**, 10.1029/2002JC001511 (2003).
 27. A. E. Gill, *Atmosphere-Ocean Dynamics* (Academic Press, San Diego, CA, 1982).
 28. W. S. Kessler, J. P. McCreary, *J. Phys. Oceanogr.* **23**, 1192 (1993).
 29. M. Tsuchiya, L. D. Talley, *J. Mar. Res.* **54**, 541 (1996).
 30. The Argo data were provided by the Argo project (www.argo.ucsd.edu). The interpolated OLR and NCEP reanalysis data were provided by NOAA/Earth System Research Laboratory, Physical Sciences Division, Boulder, Colorado (www.cdc.noaa.gov). P.S. was funded by the University of East Anglia and the Thai government. We thank N. Gillett and two anonymous reviewers for comments on the manuscript.

Supporting Online Material
www.sciencemag.org/cgi/content/full/318/5857/1765/DC1
 Materials and Methods
 Fig. S1
 References

2 July 2007; accepted 12 October 2007
 10.1126/science.1147312

Asymmetric Mating Interactions Drive Widespread Invasion and Displacement in a Whitefly

Shu-Sheng Liu,^{1*} P. J. De Barro,² Jing Xu,¹ Jun-Bo Luan,¹ Lian-Sheng Zang,¹ Yong-Ming Ruan,¹ Fang-Hao Wan³

The role of behavioral mechanisms in animal invasions is poorly understood. We show that asymmetric mating interactions between closely related but previously allopatric genetic groups of the whitefly *Bemisia tabaci*, a haplodiploid species, have been a driving force contributing to widespread invasion and displacement by alien populations. We conducted long-term field surveys, caged population experiments, and detailed behavioral observations in Zhejiang, China, and Queensland, Australia, to investigate the invasion process and its underlying behavioral mechanisms. During invasion and displacement, we found increased frequency of copulation leading to increased production of female progeny among the invader, as well as reduced copulation and female production in the indigenous genetic groups. Such asymmetric mating interactions may be critical to determining the capacity of a haplodiploid invader and the consequences for its closely related indigenous organisms.

Biological invasions threaten agricultural and natural systems throughout the world (1). Invasive animals often thrive at the expense of indigenous, closely related organisms, and insight into the causes of animal invasions often hinges on detailed assessments of

behavioral mechanisms (2). Closely related species often have incompletely isolated mate recognition systems conducive to reproductive interactions and interference (3), but rarely have such behavioral mechanisms been isolated and tested in an experimental setting to reveal their contribution to invasion biology (1). Here, we combined long-term field monitoring, caged population studies, and detailed behavioral observations to investigate the mechanisms underlying the widespread, rapid invasion by a genetic group of the whitefly *Bemisia tabaci* (Gennadius) (Hemiptera: Aleyrodidae).

The whitefly *B. tabaci*, a haplodiploid species, is a genetically diverse group including many morphologically indistinguishable populations that differ in biological characteristics but display clear geographic distributions, with indigenous

¹Institute of Insect Sciences, Zhejiang University, Hangzhou 310029, China. ²CSIRO Entomology, 120 Meiers Road, Indooroopilly, Queensland 4068, Australia. ³Institute of Plant Protection, Chinese Academy of Agricultural Sciences, Beijing 100081, China.

*To whom correspondence should be addressed. E-mail: shshliu@zju.edu.cn

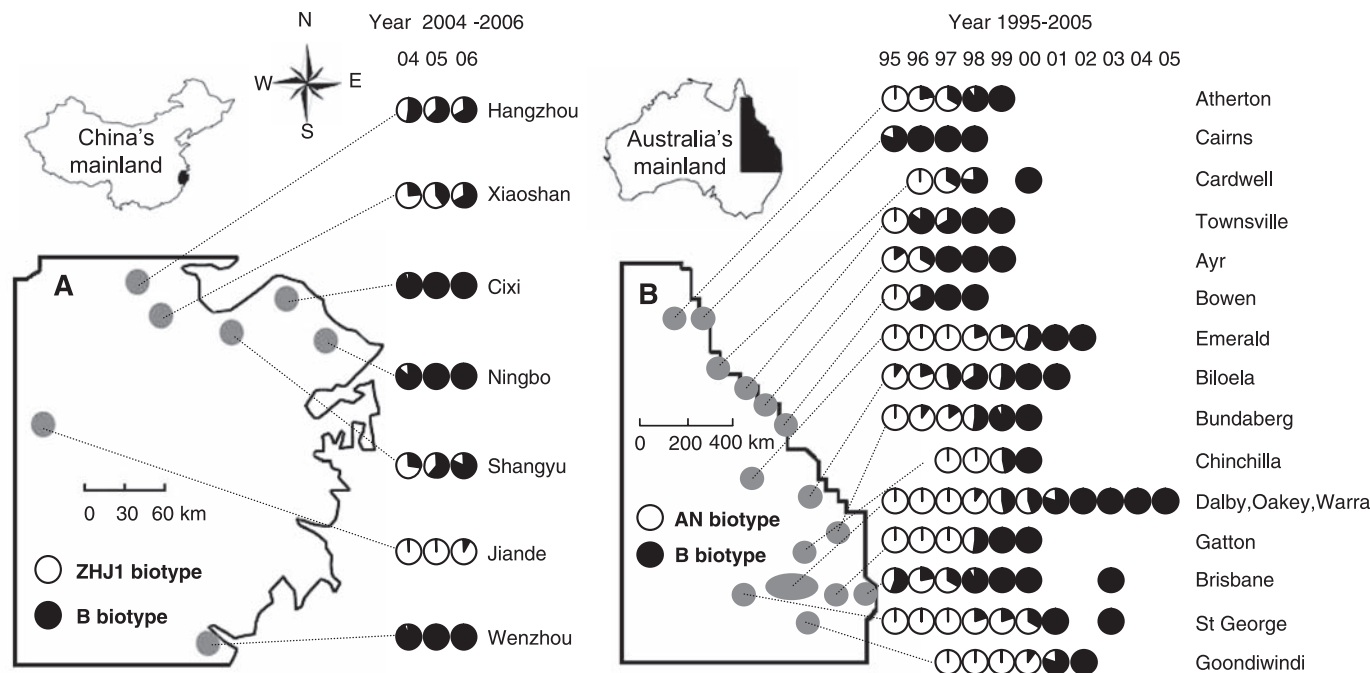


Fig. 1. Changes of the mean proportions of the exotic B biotype and indigenous biotypes of *Bemisia tabaci* after introduction of B. (A) ZHJ1 versus B on cotton at seven locations in Zhejiang, China, from 2004 to 2006. The map covers the area 122°E to 119°E from east to west and 27°30'N to 30°N from south to north. Of the seven locations, Jiande is in a western mountainous area with less transport activity relative to the

other six locations along the east coast, where transport of vegetables and ornamental plants is frequent. (B) AN versus B on *Sonchus oleraceus* at 17 locations in Queensland, Australia, from 1995 to 2005. The map covers the area 153°30' E to 142°E from east to west and 34°S to 14°40' S from south to north. Data from the other 17 locations are not depicted because of space.